AD-757 508

POST-DOCTORAL RESEARCH IN SEISMOLOGY

Frank Press, et al

Massachusetts Institute of Technology

Prepared for:

Air Force Office of Scientific Research

27 November 1972

Department of Earth and Planetary Sciences

Massachusetts Institute of Technology

Cambridge, Massachusetts 02139

POST-DOCTORAL RESEARCH IN SEISMOLOGY

Annual Report to

Air Force Office of Scientific Research

1 July 1971 - 30 June 1972

ARPA Order No. - 1827-3

Program Code - 3F10

Name of Contractor - Massachusetts Institute of Technology

Effective Date of Contract - 1 July 1966

Contract Expiration Date - 31 August 1973

Amount of Contract - $407,855

Contract No. - AF49(638)-1763

Principal Investigators - Frank Press, 617/253-3382
M. Nafi Toksöz, 617/253-6382

Program Manager - William J. Best, 202/694-5456

Short Title of Work - Post-Doctoral Research in Seismology

Sponsored by

Advanced Research Projects Agency

ARPA Order No. 1827-3

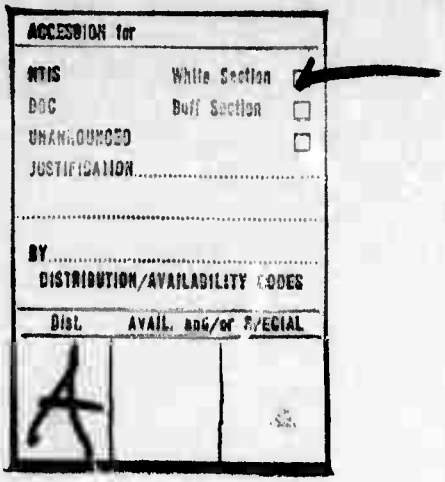

Qualified requestors may obtain additional copies from the Defense Documentation Center. All others should apply to the National Technical Information Service.

Approved for public release, distribution unlimited.

DOCUMENT CONTROL DATA - R & D

(Security classification of title, body of abstract and indexing annotation must be entered when the overall report is classified)

1. ORIGINATING ACTIVITY (Corporate author)
Massachusetts Institute of Technology
Department of Earth & Planetary Sciences
Cambridge, Massachusetts 02139

2a. REPORT SECURITY CLASSIFICATION
UNCLASSIFIED

2b. GROUP

3. REPORT TITLE

POST-DOCTORAL RESEARCH IN SEISMOLOGY

4. DESCRIPTIVE NOTES (Type of report and inclusive dates)
Scientific. ---------- Interim.

5. AUTHOR(S) (First name, middle initial, last name)
Frank Press
M. Nafi Toksöz
D.J. Andrews

6. REPORT DATE
27 November 1972

7a. TOTAL NO. OF PAGES
46

7b. NO. OF REFS
19

8a. CONTRACT OR GRANT NO
AF49(638)-1763

b. PROJECT NO.
1827-3

c.

d.

9a. ORIGINATOR'S REPORT NUMBER(S)

9b. OTHER REPORT NO(S) (Any other numbers that may be assigned this report)
AFOSR - TR - 73 - 0484

10. DISTRIBUTION STATEMENT

Approved for public release, distribution unlimited.

11. SUPPLEMENTARY NOTES

TECH, OTHER

12. SPONSORING MILITARY ACTIVITY

AFOSR (NPG)
1400 Wilson Blvd.
Arlington, Virginia 22209

13. ABSTRACT

Observations and theoretical models have been carried out to study source properties of earthquakes and explosions and structure and dynamics of the crust and upper mantle.

Earthquake sources and the structure of the crust have been studied using seismic travel times and spectral ratios.

Nonlinear propagation of waves from underground explosions has been studied numerically.

Numerical methods for tectonic flow have been developed and applied to the dynamics of mid-ocean ridges.

Ia

DD FORM 1 NOV 68 1473

14. KEY WORDS	LINK A		LINK B		LINK C	
	ROLE	WT	ROLE	WT	ROLE	WT
Crustal structure						
Inelastic wave propagation						
Numerical simulation						
Sea-floor spreading						
Seismic sources						
Seismology						

Ib

TABLE OF CONTENTS

I.

INTRODUCTION

This report summarizes research carried out under the Post-Doctoral Program in Seismology during the period 1 July 1971 to 30 June 1972 and earlier work that was submitted for publication during this period. Staff members of the Department of Earth and Planetary Sciences and Lincoln Laboratory participated in this program.

The work described here is divided into three categories: (1) properties of seismic sources, (2) studies of the dynamical behavior of the crust and upper mantle, and (3) observations of crustal structure.

The focal depths of the three largest earthquakes in the Parkfield, California, sequence were determined using first and second P arrivals at Berkeley, California. Data were insufficient to determine whether the second arrival corresponds to refraction along a discontinuity within the crust or to a complicated source-time function. With either interpretation, however, the focal depths for the three earthquakes apparently increased with time through the sequence.

Numerical calculations have been made of spherical wave propagation due to explosions in a number of rock types. The effect on the seismic source-time function of small nonlinear

irreversibility is examined for propagation at distances where the response is commonly regarded as elastic. Amplitude of long-period components is found to increase due to non-linear coupling between frequencies.

A numerical simulation of upper mantle convection has been constructed using a two-dimensional time-dependent model that allows large viscosity variations. The method has been applied to sea-floor spreading with the objective of examining the driving mechanism of mid-ocean ridges. Counterflow below the plates is confined to depths less than 340 km. It is found that for a spreading velocity of 1.2 cm/yr, the ridge can produce compressive stress in the lithosphere out to a distance of 1600 km. For a spreading rate of 6 cm/yr, however, this model is clearly excluded for it requires an excessively large stress in the lithosphere. Therefore, upwelling material must cross the seismic discontinuity at the 400 km depth.

A numerical method for more general rheological models has also been developed.

The crustal structure beneath LASA has been investigated using the spectral ratio of vertical-to-horizontal displacements of long-period P waves. The period of the lowest frequency peak in the spectral ratio, related to the vertical P wave travel-time in the crust, is quite variable over the

area spanned by the array. Variations in crustal thickness of about 7 km are implied. The Moho generally shoals from the northeast to the southwest across the array and exhibits a synclinal structure with the axis plunging toward the northeast in the southwest quadrant of LASA.

Some of the work discussed herein has already been published. The summary for such work is given below in abstract form. The complete results may be found by consulting the appropriate reference given in Section V. of this report.

II. SEISMIC SOURCES

II.1 Focal Depths of the 1966 Parkfield, California, Earthquakes by William H. Bakun (Abstract)

Differences in arrival times of seismic phases at Berkeley, California (BRK), $\Delta \sim 270$ km, for the 0408 UT June 28 ($M = 5.1$), 0426 UT June 28 ($M = 5.5$), and 1953 UT June 29 ($M = 5.0$) 1966 Parkfield, California, earthquakes imply that focal depths for these three largest events of the 1966 Parkfield sequence increased with time through the sequence. The data available are not sufficient to determine whether the observed secondary arrivals at BRK result from a slower propagation path or are part of a complicated source-time function.

II.2 Propagation of Underground Explosion Waves in the Nearly-Elastic Range by D.H. Andrews and Seymour Shlien

Abstract

The effect of small anelasticity on the propagation of spherically symmetrical waves is examined with numerical calculations. The type of anelasticity used is static hysteresis with nominal Q value of 100. Linear theories do not apply in this case. Fourier components of different frequencies do not propagate independently, but energy is transferred to lower frequencies. The extent to which reduced displacement potential is not invariant with respect to radius is examined for explosions in granite, salt, and shale.

In this paper nonlinear effects on propagation of pulses from underground explosions are examined in the nearly elastic region. The calculational method used is similar to numerical methods used in AEC laboratories (Rodean, 1971) for propagation in the close-in region, where pulse widths change from microseconds to milliseconds. We are concerned with propagation beyond the radius at which the material response is commonly considered to be elastic, and will consider the effect of small, but permanent, irreversible strains.

The mechanism of attenuation in crustal rocks has been reviewed by Knopoff (1964) and by Gordon and Davis (1968). They find that in polycrystalline samples the stress-strain path is not reversible, but has a small hysteresis that is nearly independent of strain rate. This effect is not plasticity in the usual sense, for the loading and unloading slopes are only slightly different. The effect probably arises from friction at grain boundaries.

Knopoff and MacDonald (1958) and Carpenter (1966) have developed linear viscoelastic models for which Q is constant over a broad frequency band. These models are rather complicated. Their work was motivated by trying to maintain the principle of superposition, so that wave propagation could be treated analytically. However, it is possible that a constant Q could be due to static hysteresis. This is the most plausible type of hysteresis if the energy loss is due

to friction at grain boundaries.

Johnson (1955) measured the response of an assembly of elastically loaded bodies with some sliding at their interfaces, and found a stress-strain hysteresis loop that was the same even when frequency approached zero.

In the case of static hysteresis, the principle of superposition does not hold, and different frequency components will not propagate independently. For waves from underground explosions, energy transfer from higher to lower frequencies could be important.

Since we wish to calculate wave propagation with nonlinear material properties, a numerical method must be used. We adopt the finite difference equations of Wilkins (1964) in which the first principle equations for continuum motion are approximated directly. These equations for the case of spherical symmetry are given in the Appendix.

In the material model used, the shear response is irreversible, as shown in Figure 1. The hysteresis is independent of strain rate. When shear stress and shear strain rate have the same sign (loading), a constant shear modulus μ_0 is used. When the stress and the strain rate have opposite signs (unloading), stress increments are related to strain increments using a variable shear modulus,

$$\mu = \mu_0 + \Delta\mu \frac{s}{s_{max}} \qquad (1)$$

where s_{max} is the maximum shear stress reached at the partic-

ular locality in the previous loading. Therefore, the initial unloading slope is larger than the loading slope, and then decreases smoothly to the same value. Behavior is similar for loading and unloading in the opposite direction. In this model the residual strain when stress is reduced to zero is proportional to the maximum stress reached. The relative energy loss is independent of amplitude and of frequency. The principle of superposition does not apply.

We will calculate spherical wave propagation for the explosions, Gasbuggy, 29 kilotons detonated in shale, Hardhat, 5 kilotons in granite, and Salmon, 5 kilotons in salt. In each case the waveform is specified at a radius beyond the strongly inelastic region, and propagation to greater distances is calculated. It is not reasonable to assume that the material is the same at these distances as at the shot point. The Pictured Cliffs Sandstone formation in which a Gasbuggy gauge was located is chosen as a typical near surface crustal rock. Its properties are used in all calculations. Density is 2.51 gm/cm^3, P wave velocity is 4.3 km/sec, and Poisson's ratio is 0.3 (Perret, 1969). In the inelastic calculations, the shear modulus was calculated from equation (1) with $\mu_0 = 0.1327$ megabar and $\Delta\mu = 0.0328$ megabar. This corresponds to a relative energy loss in shear of 16%, or in uniaxial strain of 6%, giving a nominal Q for P waves of 100.

The Gasbuggy waveform at 468 meters, with a peak velocity of 2.4 meter/sec, peak displacement of 6.8 cm, and final displacement of 2.6 cm, (Perret, 1969) can be matched roughly (in the elastic case) by a stress pulse of the form

$$\Sigma_\tau = p_0 + p_1 e^{-t/\tau} \qquad (2)$$

For the Gasbuggy calculations units of length and time are scaled down by the factor $(5/29)^{1/3}$, so that all calculations are for 5 kilotons. Values of the parameters in equation (2) for Gasbuggy scaled to 5 kilotons are given in Table I. The Salmon waveform at 625 meters, with a peak velocity of 2 meter/sec, peak displacement of 2.8 cm, and final displacement of 0.85 cm (Patterson, 1964) is also fit by a stress pulse of the form given in equation (2) with parameters listed in Table I.

The Hardhat calculation is not based on a measured waveform. There was a significant amount of tectonic strain release in the Hardhat event (Toksoz and Kehrer, 1971), which could have contributed to the measured displacement. Our calculation is based on the stress pulse calculated by Cherry (Rodean, 1971), which can be fit closely by equation (2) with parameters listed in Table 1.

In order to facilitate comparison of attenuation over equal distances, it was decided to do all the numerical calculations with the input waveform imposed at the same radius, 400 meters. The stress profiles specified in Table 1

are transformed by varying p_0 inversely with the cube of radius to get the same final displacement and varying p_1 inversely with radius to get the same peak velocity as a function of radius in the elastic case. The transformed parameters are listed in Table II.

Although this transformation of the stress pulse keeps peak velocity and final displacement invariant, it changes the spectrum of the wave generated. In the elastic case the period of the predominant low frequency component is proportional to the radius at which the stress pulse of equation (2) is applied (Sharpe, 1942). We have not taken care to establish realistically the radii at which the three different explosion pulses become nearly elastic, but we will investigate the effect of nonlinear material response on three waveforms with varying ratio of impulse to step function.

For each explosion an elastic and an inelastic calculation was done. In the elastic calculations, the stress pulse specified in Table II was applied at 400 meters. The calculated method was checked by verifying that the reduced displacement potentials calculated at different radii were the same. Velocity as a function of time at [illegible] meters was saved from each of the elastic calculations and was used as a boundary condition for the inelastic calculations. The finite difference zone size in all calculations was 5 meters.

Velocity pulses calculated for Gasbuggy at a radius of 1.4 km are compared in Figure 2. The waveform for the inelastic case looks similar to the elastic waveform but has smaller amplitude. An important feature not evident in this figure is that the final displacement is larger in the inelastic case.

Reduced displacement potential is calculated from the equation

$$\Psi(t) = cr \int_0^t d(t') e^{c(t-t')/r} dt' \qquad (3)$$

where d is displacement. Potentials for the three explosions in the case of elastic propagation beyond 400 meters are shown as solid curves in Figure 3.

In the inelastic case the reduced displacement potential has no meaning, although the integral in equation (3) can be performed. Indeed, this is what is done when a "reduced displacement potential" is derived from measurements, for there is no assurance that the material response is strictly elastic. In the inelastic calculations Ψ calculated from equation (3) at 400 meters is the same as the elastic case, since displacement is prescribed to be the same there. At greater distances, however, Ψ is not the same. Dashed curves in Figure 3 show Ψ for the three explosions at 1.4 km. The difference between the solid and dashed curves is the difference that might be expected in "potentials" derived from measurements 1 km apart for spherical wave propagation in

rock with Q = 100. The initial peak of Ψ is smaller due to attenuation of the propagating pulse, but then Ψ rises to larger values because of the larger final displacement.

These inelastic "reduced displacement potentials" can not be rigorously related to more distant seismic waves, but some qualitative conclusions can be drawn. If the material had been changed from inelastic to elastic at 1.4 km, the reduced displacement potential calculated there would have been rigorously meaningful. In this case the initial peak of Ψ would not change much, since it is determined by attenuation within 1.4 km. Later values of Ψ would be smaller since the final displacement is determined by yielding both within and beyond 1.4 km. However, these later value of Ψ would still be larger than in the all elastic case.

The functions shown in Figure 3 are analyzed here as if they were truly seismic source-time functions. Particle velocity of surface waves and head waves is proportional to the first derivative of Ψ. Fourier amplitude spectra of $d\Psi/dt$ are shown in Figure 4 for the elastic and inelastic cases at 1.4 km for the three explosions. The location of the spectral peak near 2 hertz is determined by the choice of 400 meters as the cavity radius. At this frequency and above the amplitude in the inelastic cases is reduced due to attenuation through 1 km of irreversible material. The

The DC component is larger due to the larger final displacement. This would not be the case with a linear viscoelastic attenuation model. Since the principle of superposition does not apply in this model, different components do not propagate independently. Energy can be transferred from higher to lower frequencies. In the spectra shown it is evident that the increased energy in the DC component is taken from the 1 hertz component. This minimum might change as the wave propagates farther.

The particle velocity of distant body waves is proportional to the second derivative of Ψ. Therefore, body wave spectra are obtained by multiplying surface wave spectra by frequency. Therefore, the inelastic effects at low frequency will be less dramatic for body waves than for surface waves.

The quality factor, Q, of 100 used here is reasonable for near-surface crustal rocks. Also, static hysteris is consistent with laboratory measurements. The fact that static hysteresis has not been considered before in seismological theory is related more to difficulty of analysis than to indications of the data. Therefore, the inelastic model used here is a reasonable possibility. The seismic source-time function for an underground explosion can be significantly different from that derived at the commonly accepted elastic radius.

ACKNOWLEDGEMENT

This research was supported by the Advanced Research Projects Agency and monitored by the Air Force Office of Scientific Research under contract AF 49(638) - 1763.

REFERENCES

Carpenter, E.W. (1966), Absorption of elastic waves--an operator for a constant Q mechanism, British Report AWRE-0-43/66.

Gordon, R.B., and L.A. Davies (1968), Velocity and attenuation of seismic waves in imperfectly elastic rock, J. Geophys. Res.13, 3917-3935.

Johnson, K.L. (1955), Surface interaction between elastically loaded bodies under tangential forces, Proc. Roy. Soc. London A230, 531.

Knopoff, L. (1964), Q, Reviews of Geophys. 2, 625-657.

Knopoff, L. and G.J.F. MacDonald (1958), Attenuation of small amplitude stress waves in solids, Rev. Mod. Phys. 30, 1178.

Patterson, D.W. (1966), Nuclear decoupling, full and partial, J. Geophys. Res. 71, 3427.

Perret, W.R. (1969), Gasbuggy Seismic source and surface motion, U.S. Atomic Energy Commission, PNE-1002.

Rodean, H.C. (1971), Nuclear-explosion seismology, U.S. Atomic Energy Commission, Oak Ridge, Tennessee.

Sharpe, J.A. (1942), The production of elastic waves by explosion pressures. I. Theory and empirical field observations, Geophysics 7, 144-154.

Toksöz, M.N. and H.H. Kehrer (1971), Underground explosions: Tectonic utility and dangers, Science, 173, 230-233.

Wilkins, M.L. (1964), Calculation of elastic plastic flow, Methods in Computation of Physics Vol. 3, Adler, Fernbach, Rotenberg, Ed. Academic Press, New York.

TABLE 1

	Radius	p_0	p_1	τ
Gasbuggy (scaled)	260 m	29.7 bar	259 bar	15.7 msec
Hardhat	400	11	144	10
Salmon	625	7.2	215	14.1

TABLE II

	Radius	p_0	p_1	τ
Gasbuggy (scaled	400 m	8.15 bar	168 bar	15.7 msec.
Hardhat	400	11	144	10
Salmon	400	27.5	336	14.1

Figure Captions

Figure 1: A typical path for shear stress versus shear strain for the inelastic model.

Figure 2: Particle velocity at 1.4 km for the Gasbuggy calculations. Solid curve is the elastic case and dashed curve is the inelastic case.

Figure 3: Solid curves are reduced displacement potentials for the three explosions in the elastic case. Dashed curves are functions derived by equation (3) from displacement at 1.4 km in the inelastic case.

Figure 4: Fourier amplitude spectra of surface wave source time functions. Solid curves are the elastic case. Dashed curves are found by taking dashed curves of Fig. 3 as reduced displacement potentials.

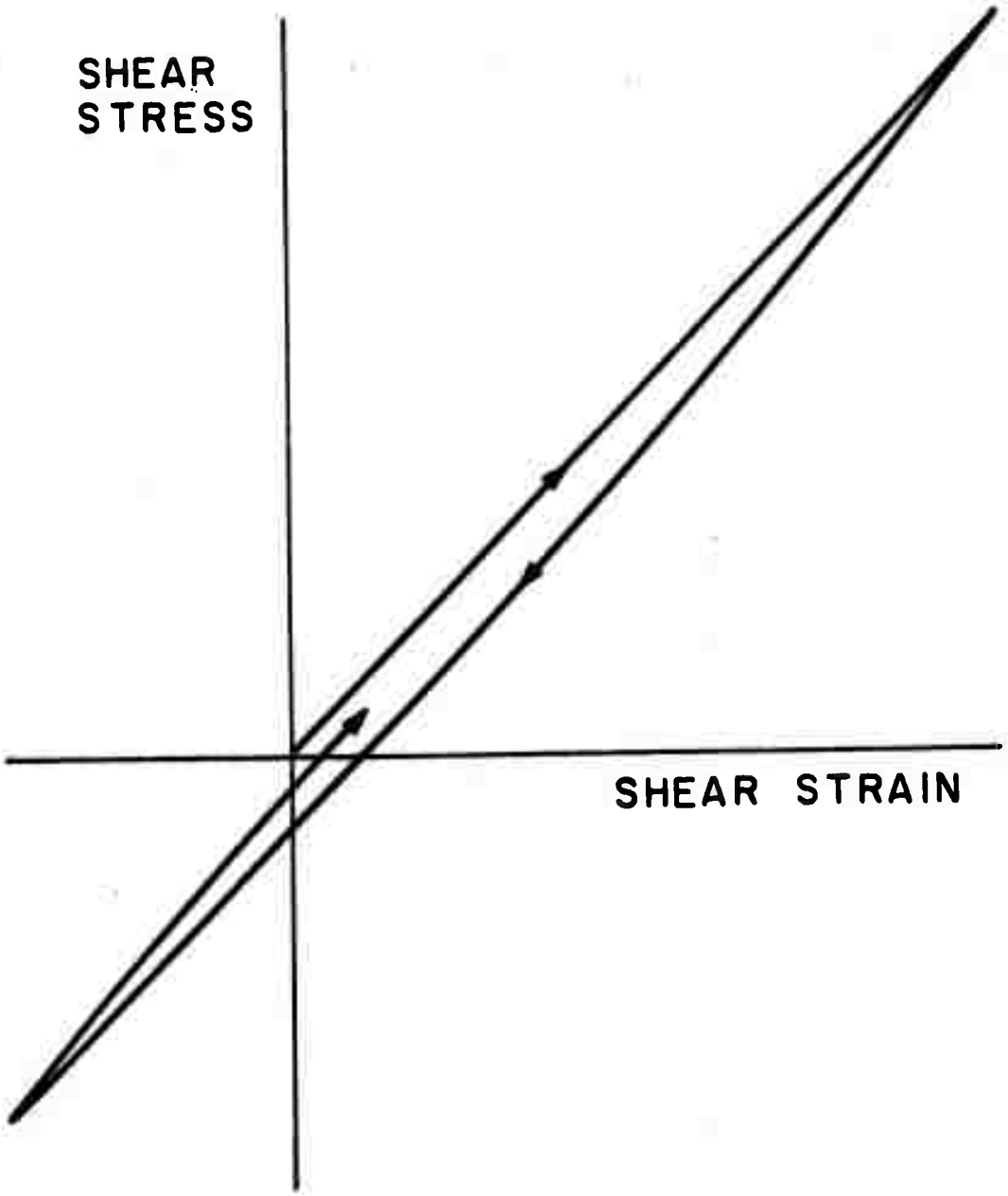
SHEAR
STRESS
SHEAR STRAIN

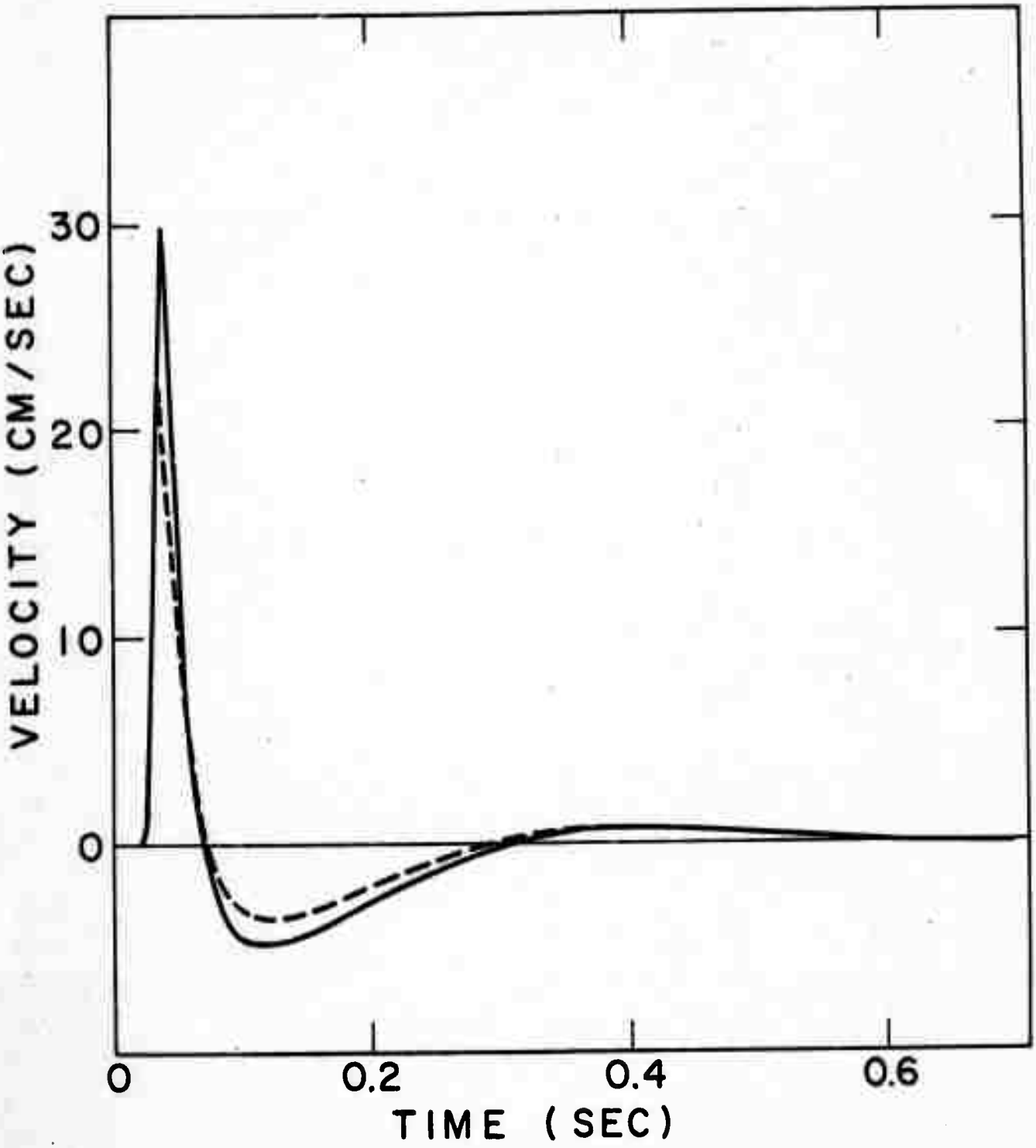
VELOCITY (CM/SEC)
30
20
10
0
0
0.2
0.4
0.6
TIME (SEC)

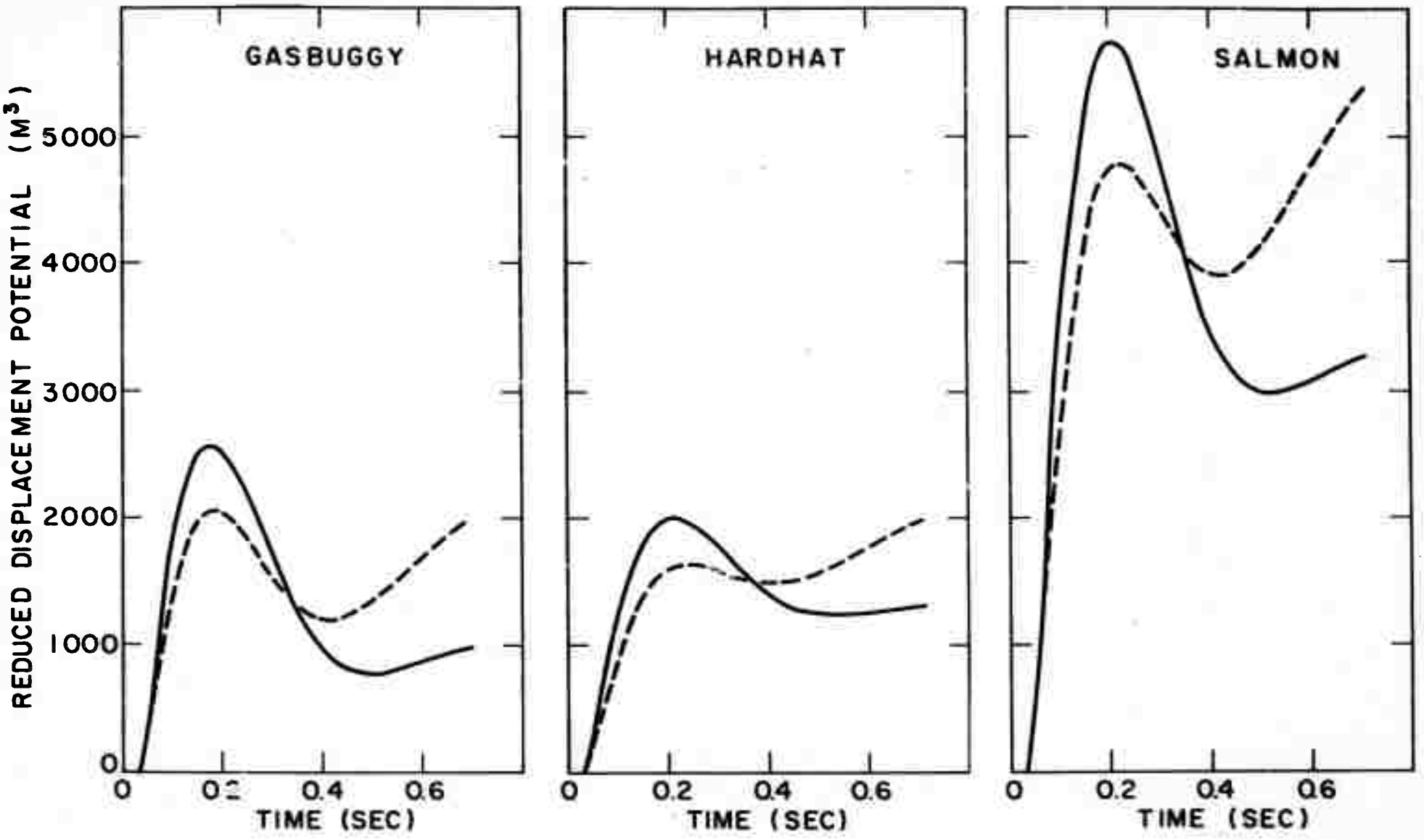
GASBUGGY
HARDHAT
SALMON
REDUCED DISPLACEMENT POTENTIAL (M³)
5000
4000
3000
2000
1000
0
0
0.2
0.4
0.6
TIME (SEC)

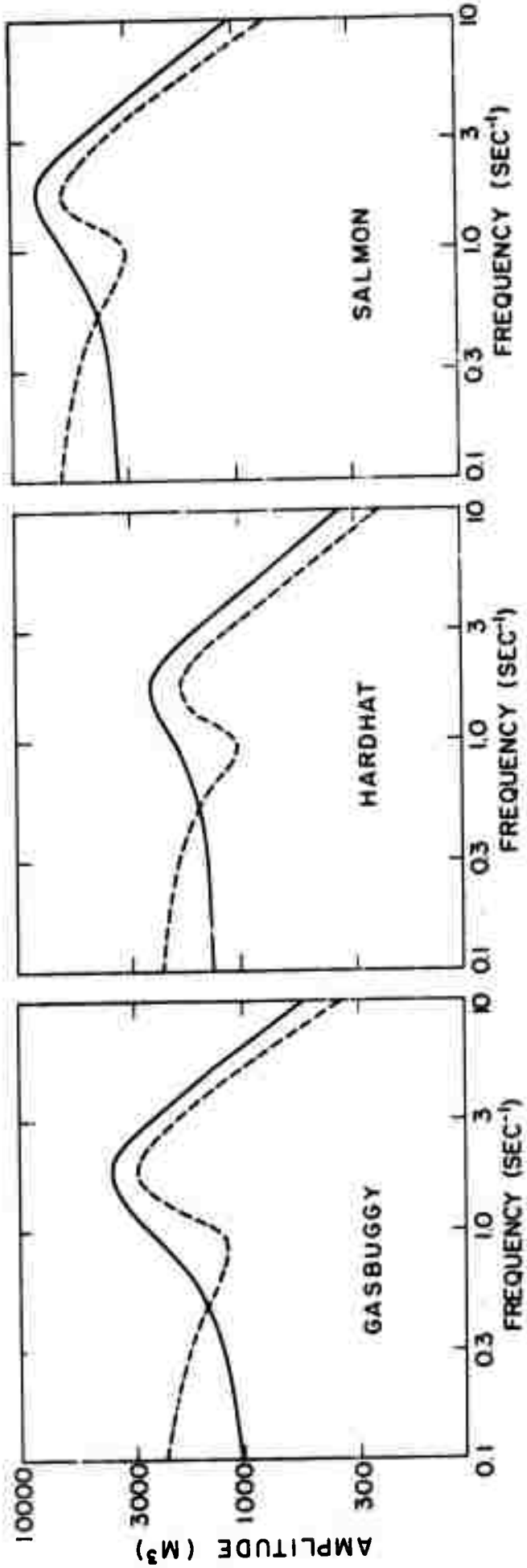
AMPLITUDE (M³)
10000
3000
1000
300
GASBUGGY
HARDHAT
SALMON
0.1
0.3
1.0
3
10
FREQUENCY (SEC⁻¹)

APPENDIX

A Lagrangian finite difference scheme is used. Space intervals are indexed by the subscript j and time steps are indexed by the superscript n. Grid points move with the material, so that each interval between points always contains the same mass.

The equation of motion

$$\frac{\partial u}{\partial t} = \frac{1}{\rho}\frac{\partial \Sigma_r}{\partial r} + 2\frac{\Sigma_r - \Sigma_\theta}{\rho\ r}$$

is approximated by the finite difference equation

$$\dot{u}_j^n = [(\Sigma_r)_{j+1/2}^n - (\Sigma_r)_{j-1/2}^n]/\phi_j^n + 2\beta_j^n$$

where

$$\phi_j^n = 1/2\left[\rho_j^n + 1/2(r_{j+1}^n - r_j^n) + \rho_{j-1/2}^n(r_j^n - r_{j-1}^n)\right]$$

$$\beta_j^n = 1/2\left[\frac{(\Sigma_r)_{j+1/2}^n - (\Sigma_\theta)_{j+1/2}^n}{1/2\ \rho_{j+1/2}^n(r_{j+1}^n + r_j^n)} + \frac{(\Sigma_r)_{j-1/2}^n - (\Sigma_\theta)_{j-1/2}^n}{1/2\ \rho_{j-1/2}^n(r_j^n + r_{j-1}^n)}\right]$$

Then acceleration is integrated to update velocity

$$u_j^{n+1/2} = u_j^{n-1/2} + \Delta t\ \dot{u}_j^n$$

and the velocity is integrated to update the radius of each Lagranian point

$$r_j^{n+1} = r_j^n + \Delta t\ u_j^{n+1/2}$$

Updated velocities and co-ordinates are used to evaluate strain rates.

$$(\dot{\varepsilon}_r)^{n+1/2}_{j+1/2} = \frac{u^{n+1/2}_{j+1} - u^{n+1/2}_{j}}{r^{n+1/2}_{j+1} - r^{n+1/2}_{j}}$$

$$(\dot{\varepsilon}_\theta)^{n+1/2}_{j+1/2} = \frac{u^{n+1/2}_{j+1} + u^{n+1/2}_{j}}{r^{n+1/2}_{j+1} + r^{n+1/2}_{j}}$$

$$(\frac{\dot{V}}{V})^{n+1/2}_{j+1/2} = (\dot{\varepsilon}_r)^{n+1/2}_{j+1/2} + 2(\dot{\varepsilon}_\theta)^{n+1/2}_{j+1/2}$$

Then a new value of pressure is found

$$P^{n+1}_{j+1/2} = P^{n}_{j+1/2} - k\,(\frac{\dot{V}}{V})^{n+1/2}_{j+1/2}\,\Delta t$$

where k is bulk modulus. Updated stress deviators are given by

$$(s_r)^{n+1}_{j+1/2} = (s_r)^{n}_{j+1/2} + 2\mu\left[(\dot{\varepsilon}_r)^{n+1/2}_{j+1/2} - \frac{1}{3}\,(\frac{\dot{V}}{V})^{n+1/2}_{j+1/2}\right]\Delta t$$

$$(s_\theta)^{n+1}_{j+1/2} = -\frac{1}{2}(s_r)^{n+1}_{j+1/2}$$

Irreversible behavior of the stress deviator s_r is obtained if the shear modulus μ used in the incremental equation above is not constant, but depends on s_r and on the direction of change of s_r.

Total stress components are

$$(\Sigma_r)^{n+1}_{j+1/2} = (-P + s_r)^{n+1}_{j+1/2}$$

$$(\Sigma_\theta)^{n+1}_{j+1/2} = (-P + s_\theta)^{n+1}_{j+1/2}$$

After this sequence of equations is executed for each value of j, the time step index n can be incremented by one and the cycle can be repeated. All equations are explicit.

The stability requirement is

$$\Delta t < \frac{\Delta r}{c}$$

where c is sound speed.

III. DYNAMICS OF THE CRUST AND UPPER MANTLE

III.1 Numerical Simulation of Sea-Floor Spreading by D.J. Andrews (Abstract)

Upper mantle convection, including lithospheric plate motion, is simulated numerically using a two-dimensional time-dependent method that allows large viscosity variations. The numerical operator developed for viscous flow is in self-adjoint form, so that the conjugate gradient iteration method may be used. Convergence is faster than with relaxation methods. The method is applied to sea-floor spreading with the objective of examining the driving mechanism of mid-ocean ridges. In accordance with this objective, deep convection is suppressed in the model. Counterflow below the plates is confined to depths less than 340 km. The model is fit to observed topography at four different ridge locations. It is found that for a spreading velocity of 1.2 cm/yr, the ridge can produce compressive stress in the lithosphere out to a distance of 1600 km. For a spreading velocity of 6 cm/yr this model is clearly excluded, for it requires excessively large stress in the lithosphere. Therefore upwelling material must cross the seismic discontinuity at 400 km depth.

III.2 A Numerical Method for Creep Deformation of Solids by D.J. Andrews

This note is concerned with extension of the procedure described by Andrews and Hancock [1] to time-dependent problems in which motion is slow enough that inertial forces are negligible. Time dependence of the solution may arise from stress relaxation of the material and from time-dependent boundary conditions. The procedure involves advancing through time in finite steps and iterating to acheive stress equilibrium at each step in time. It is discussed in terms of a Maxwellian viscoelastic model that can be generalized to nonlinear cases.

Stress components σ_{ij} are decomposed into stress deviators and pressure

$$\sigma_{ij} = s_{ij} - P\,\delta_{ij}$$

Pressure is uniquely determined by volume, but stress deviator components obey a stress relaxation law, which in differential form is

$$ds_{ij} = 2\mu\,de_{ij} - s_{ij}\,dt/\tau$$

where e_{ij} is strain deviator, μ is shear modulus, and τ is relaxation time. If τ is constant this is linear Maxwellian viscoelasticity. In nonlinear cases τ is a function of stress. To have a properly covariant description, τ should be expressed as a function of stress in-

variants.

The finite difference equation used to advance stress in one zone from time step n to step $n + 1$ is derived as follows. Let $(\dot{e}_{ij})^{n+1/2}$ be the strain deviator rate, found from velocities, for that zone for advancing from time step n to a particular iteration at time step $n + 1$. A finite difference analogue of the differential equation above is

$$(s_{ij})^{n+1} = (s_{ij})^{n} + 2\mu(\dot{e}_{ij})^{n+1/2}\,\Delta t - 1/2[(s_{ij})^{n+1} + (s_{ij})^{n}]\,\frac{\Delta t}{\tau}$$

This may be rearranged to get an explicit equation

$$(s_{ij})^{n+1} = [(s_{ij})^{n} + 2\mu(\dot{e}_{ij})^{n+1/2}\,\Delta t - 1/2(s_{ij})^{n}\,\frac{\Delta t}{\tau}]/(1 + 1/2\,\frac{\Delta t}{\tau})$$

This equation is stable for all values of Δt and is accurate to second order in $\Delta t/\tau$.

An iteration must be performed to converge to stress equilibrium at time step $n + 1$. Solution of the above equation for all zones constitutes step 4 of the iteration outlined in [1].

To proceed through the next iteration at time step $n + 1$, stress components just calculated are used to find the unbalanced force on each grid point (step 1 of the iteration). Then, grid points are displaced in the direction of this force to go from positions in the previous iteration at time step $n + 1$ to positions in the current iteration at time step $n + 1$ (step 2). The velocities of grid points from time step n to the current iteration in time step $n + 1$, are found. From these velocities strain rates are found (step 3), and then the stress calculation may be repeated.

In the case of nonlinear stress relaxation, the relaxation time τ should be evaluated from invariants of the stress tensor averaged at the new and old times. In this average one may use stress at time step n and stress from the previous iteration at time step $n + 1$.

This procedure has been used in a problem with a cubic creep law. The iteration behaved in a reasonable way.

To check the accuracy of the method a problem was done with a linear viscoelastic material in an infinite half space, with a pressure applied to the surface. The x-axis extends into the medium and the surface is at $x = 0$. The material has been at rest with no pressure on the surface at all times up to $t = 0$. At $t = o$ the pressure

$$p = P \cos \alpha y$$

is suddenly applied to the surface and is held constant thereafter. The analytic solution is found by applying Bland's correspondence principle [2] to the elastic solution [3]. The components of displacement are

$$u = \frac{P}{2\mu\alpha} e^{-\alpha x} \cos \alpha y \left[- \frac{\mu}{k} (1 - a) e^{-at/\tau} + \frac{\mu}{k} + 1 + \alpha x + (1 + \alpha x) t/\tau \right]$$

and

$$v = - \frac{P}{2\mu\alpha} e^{-\alpha x} \sin \alpha y \left[- \frac{\mu}{k} (1 - a) e^{-at/\tau} + \frac{\mu}{k} - \alpha x - \alpha x \, t/\tau \right]$$

where k is bulk modulus and

$$a^{-1} = 1 + \mu/(3k)$$

At $t = 0$ these expressions are the solution for the elastic case [3]. Note that in the elastic case the horizontal displacement reverses direction at a depth

$$\alpha x = 1 - 2\nu \, ,$$

while in the viscoelastic solution the horizontal velocity at late times is in the same direction at all depths.

In the numerical test case we will choose $\tau = 1$, $\alpha = 1$, $2\mu = 1$, $\nu = 0.2$. The numerical method is valid for large displacements, but the analytic solution holds only for small displacements. To keep displacement small we choose $P = 10^{-4}$. Displacements are multiplied by 10^4 in the figures.

In the finite difference calculation 8 zones are used in a half wavelength of the pressure variation, and the region considered is 12 zones deep. Zones are approximately square. The pressure was suddenly applied at time zero, and the calculation proceeded for one relaxation time. The time step used was $\tau/10$. In each time step 200 iterations were performed to approach stress equilibrium. The number of iterations required for long wavelength components to converge increases when finer zoning is used. It is proportional to the square of the number of zones in one dimension.

Displacements calculated after the first time step are shown in Figure 1. This is approximately the elastic solution expected for instantaneous displacement. Variation of each component of displacement in the direction parallel to the surface is sinusoidal, as it should be, within 1 percent. Time dependence of the x-component of displacement at $y = 0$ is shown for four different depths in Figure 2. Symbols show calculated values and the solid curves are the analytic solution. In the first time step errors are 6

percent of the maximum displacement. This error could have been reduced by using a larger number of iterations. The deviation from stress equilibrium is partly corrected in the next time step, where errors are less than 2 percent of maximum displacement. Time dependence of the y-component of displacement at $y = \pi/2$ is shown in Figure 3.

ACKNOWLEDGEMENT

This work was supported by the Advanced Research Projects Agency and monitored by the Air Force Office of Scientific Research under Contract No. AF 49(638)-1763.

REFERENCES

1. D.J. Andrews and Steven L. Hancock, Journal of Computational Physics, this issue.

2. D.R. Bland, "The Theory of Linear Viscoelasticity", Pergamon Press, New York, 1960.

3. I.N. Sneddon, "Fourier Transforms", McGraw Hill, New York, 1951.

Figure 1. Displacement field in the demonstration problem after the first step in time.

Figure 2. Vertical displacement at four different depths as a function of time. Symbols are calculated values. Solid curves are the analytic solution.

Figure 3. Horizontal displacement at four different depths or a function of time. Symbols are calculated values. Solid curves are the analytic solution.

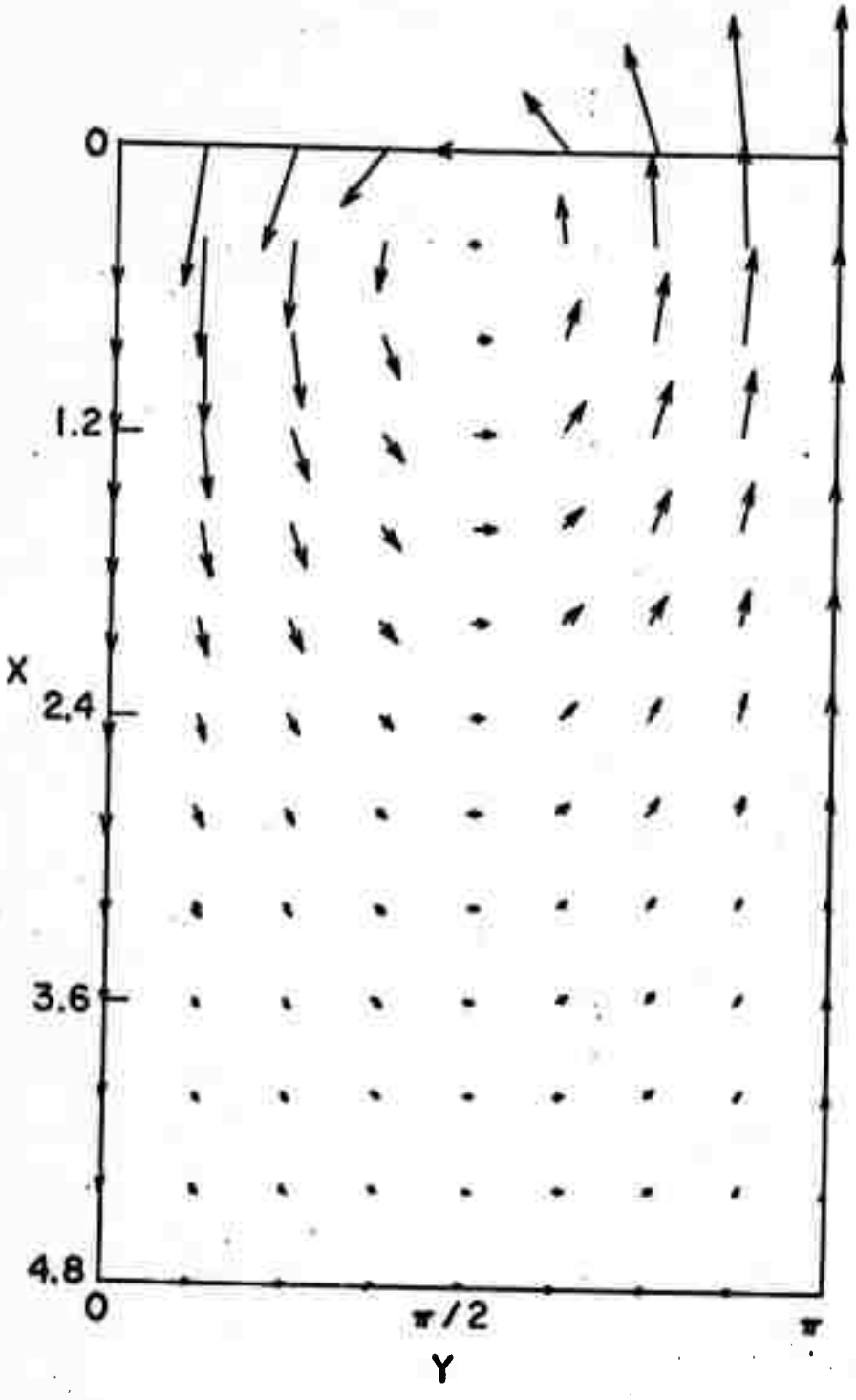
0
1.2
X
2.4
3.6
4.8
0
π/2
π
Y

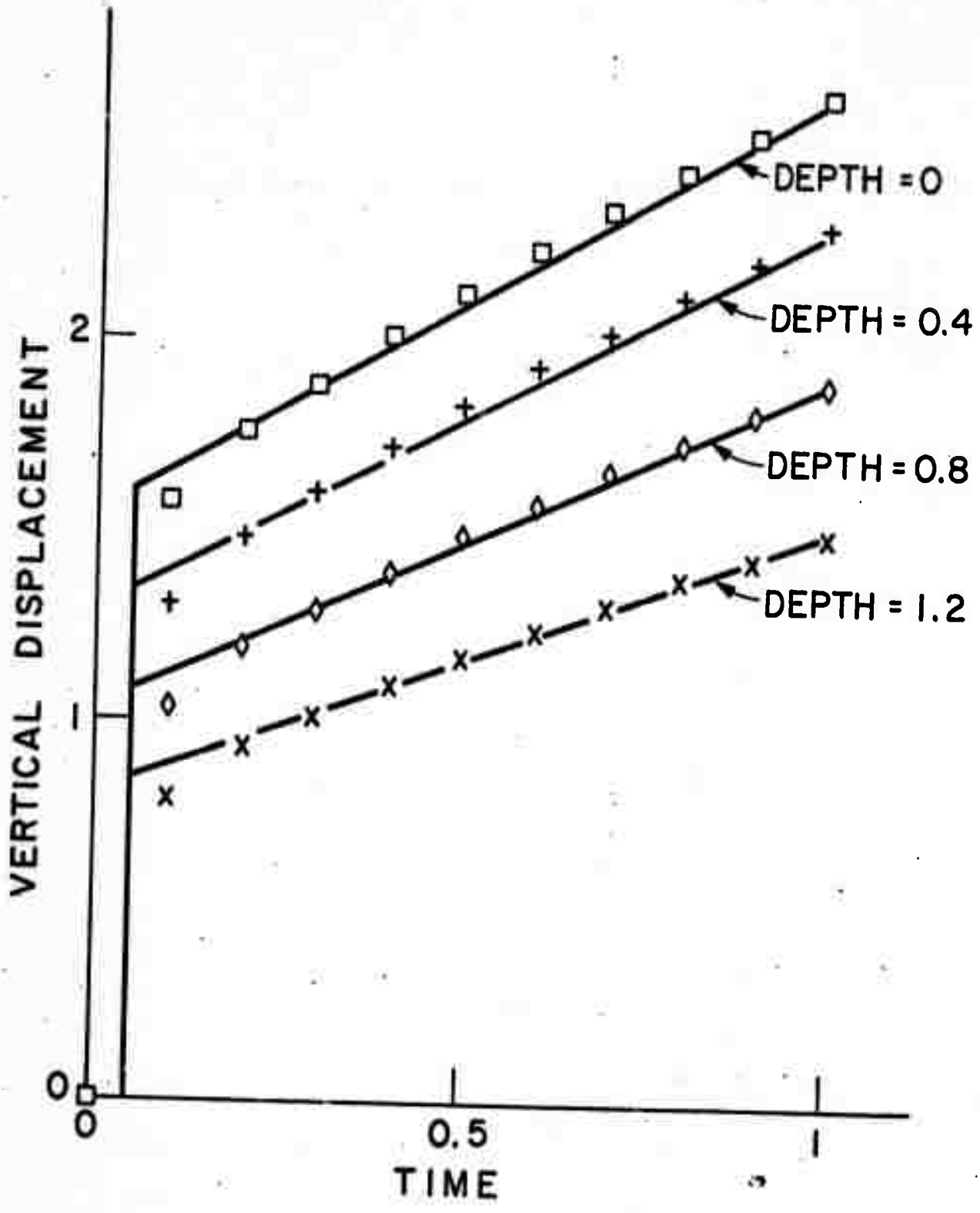
DEPTH = 0
DEPTH = 0.4
DEPTH = 0.8
DEPTH = 1.2
VERTICAL DISPLACEMENT
2
1
0
0
0.5
1
TIME

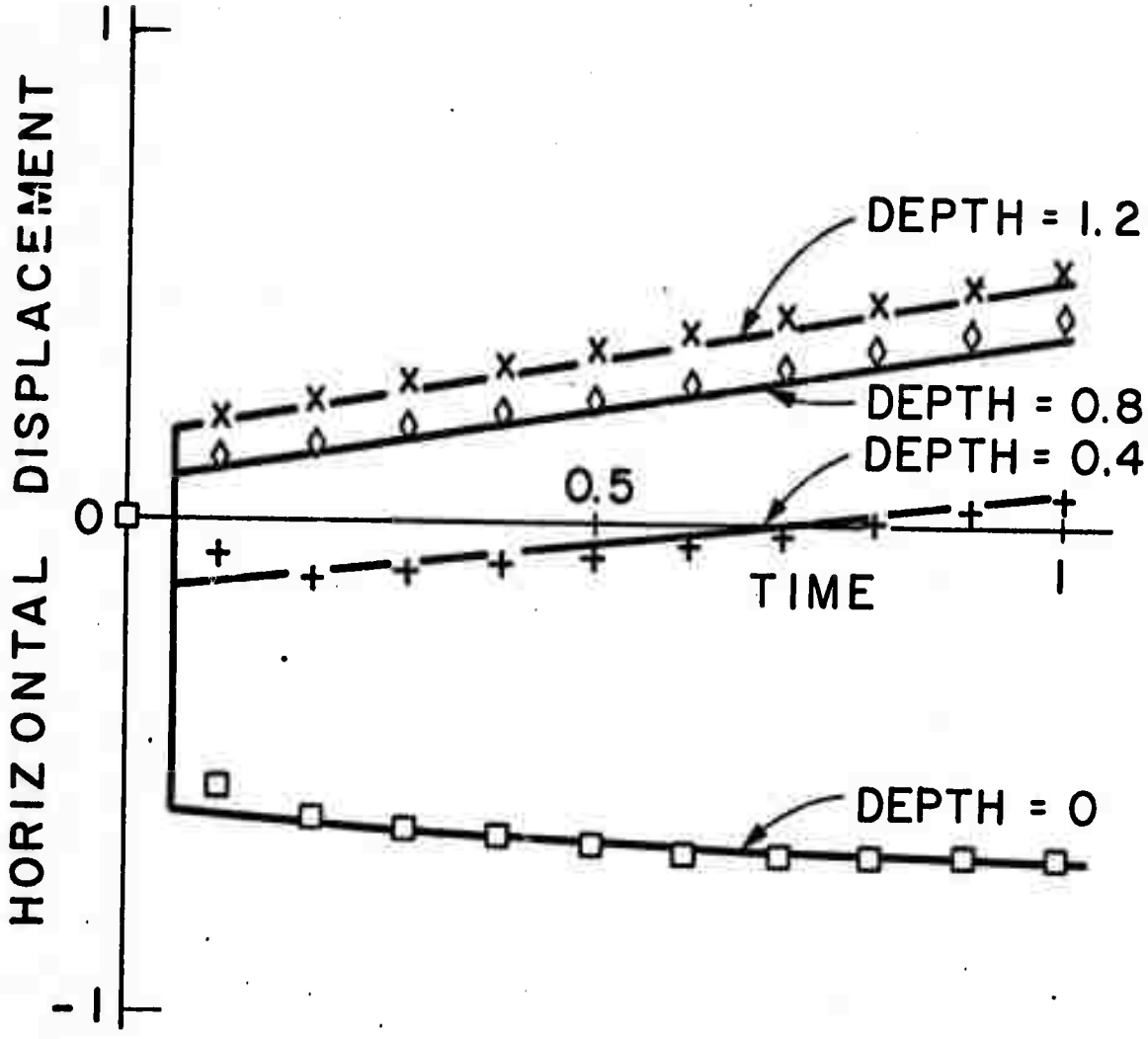
HORIZONTAL DISPLACEMENT
1
0
-1
0.5
1
TIME
DEPTH = 1.2
DEPTH = 0.8
DEPTH = 0.4
DEPTH = 0

IV. STRUCTURE OF THE CRUST

IV.1 Crustal Structure Beneath LASA from Long-Period P-Wave Spectra by William H. Bakun (Abstract)

Long-period transfer-function ratios from events in South America, Fiji-Tonga, and Japan recorded at the LASA subarray centers are interpreted in terms of Haskell-Thomson theory. The transfer-function ratio data provide a three-dimensional model for the crustal structure beneath LASA. The proposed structure can be characterized by two trends: (1) crustal thinning from the northeast to the southwest across the array and (2) a synclinal structure in the southwest quadrant of the array with axis plunging toward the northeast.

V. LIST OF PAPERS SUBMITTED FOR PUBLICATION
1 July 1971 - 30 June 1972

Andrews, D.J., Numerical simulation of sea-floor spreading, J. Geophys. Res., 77, 6470-6481, 1972.

Andrews, D.J. and S. Shlien, Propagation of underground explosion waves in the nearly-elastic range, Bull. Seism. Soc. Am., to appear December 1972.

Andrews, D.J., A numerical method for creep deformation of solids, J. Comp. Physics, to be published.

Bakun, W.H., Focal depths of the 1966 Parkfield, California, earthquakes, J. Geophys. Res., 77, 3816-3822, 1972.

Bakun, W.H., Crustal structure beneath LASA from long-period P-wave spectra, submitted to J. Geophys. Res.

VI. RESEARCH ASSOCIATE SUPPORTED BY CONTRACT NO. AF49(638)-1763

D.J. Andrews

Dr. Andrews has been a Research Associate at M.I.T. since 1970. He has been working on numerical calculations of viscous flow at mid-ocean ridges, of viscoelastic deformation of the crust, and of elastic and inelastic wave propagation. Of particular interest to this contract is his work on propagation of waves from underground explosions in the nearly-elastic range of distances. His most recent work is on near-field motion from fault dislocation and on release of tectonic stress by explosions.

Publications:

D.J. Andrews, Numerical simulation of sea-floor spreading, J. Geophys. Res., 77, 6470-6481, 1972.

D.J. Andrews and S. Shlien, Propagation of underground explosion waves in the nearly-elastic range, Bull. Seism. Soc. Am., to appear December 1972.

D.J. Andrews, A numerical method for creep deformation of solids, to be published in J. Comp. Physics.